Chemical Engineering Journal 146 (2009) 355–361

Contents lists available at ScienceDirect

Chemical Engineering Journal

journal homepage: www.elsevier.com/locate/cej

High photocatalytic activity of silver-loaded ZnO-SnO_2 coupled catalysts

Huihu Wang, Seonghoon Baek, Jonghyuck Lee, Sangwoo Lim*

Department of Chemical Engineering, Yonsei University, 134 Shinchon-dong, Seodaemoon-gu, Seoul 120-749, Republic of Korea

ARTICLE INFO

Article history:
Received 27 February 2008
Received in revised form 11 June 2008
Accepted 19 June 2008

Keywords:
Coupled oxide powders
Silver
Zinc oxide
Tin oxide
Photocatalytic activity
Methyl orange

ABSTRACT

In order to improve the photocatalytic activity of ZnO, ZnO-SnO_2 coupled catalysts and Ag/ZnO-SnO_2 catalysts with different Ag contents (1–5%) were prepared through the coprecipitation method. The samples were characterized by X-ray diffraction, UV–vis diffuse reflectance spectroscopy, specific surface area, and transmission electron microscopy combined with energy dispersive spectroscopy. The degradation rate of methyl orange shows that the photocatalytic activity of ZnO-SnO_2 coupled catalyst prepared at pH 7 was higher than that of the coupled catalyst prepared at pH 10. After Ag was loaded on the surface of coupled catalysts prepared at pH 7, the photocatalytic performance of catalysts was greatly improved. The optimum Ag loading amount was found to be around 3%. The activity of 3%Ag/ZnO-SnO_2 catalyst was higher than that of the pure ZnO catalyst and the ZnO-SnO_2 coupled catalyst prepared at pH 7 by 84 and 88%, respectively. Our study demonstrates that the combination of noble metal loading and the semiconductor coupling on the surface of a semiconductor catalyst would be an effective way to improve the photocatalytic activity of catalysts.

1. Introduction

The hazardous wastes related to industrial activities, including toxic contaminated air and organic wastewater have resulted in serious worldwide environmental problems. Semiconductor photocatalysis has attracted increasing attention over the last two decades as an effective technique to eliminate the pollutants in air and wastewater [1–3]. While many efforts have been made to put this technique into commercial application, many problems arise, such as the fast recombination rate of the photoexcited electron–hole pairs, which is the key factor in the process of semiconductor photocatalysis [3]. Therefore, there has been much interest in lowering the recombination rate of electron–hole pairs in order to improve the photocatalytic efficiency of semiconductor photocatalysts [4–7].

Coupling two semiconductor nanoparticles with different band gap widths has been demonstrated in many studies as one of the most effective ways to slow the recombination of electron–hole pairs [8–25]. In contrast to the single semiconductor photocatalyst, many coupled semiconductor systems, such as ZnO-Fe_2O_3 [8,9], ZnO-WO_3 [8,9], ZnO-SnO_2 [10–17], TiO_2-WO_3 [18,19], TiO_2-SnO_2 [20–24], TiO_2-ZnO [25], have shown high photocatalytic efficiency for increasing the charge separation and extending the energy range of photoexicitation. Furthermore, the optimal photocatalytic activities of coupled semiconductor systems have been obtained through the controlled synthesis process. As for ZnO-SnO_2 semiconductor oxides, different preparation methods have been applied, such as the coprecipitation method [10,14–17], the hydrothermal method [11,12], the grinding method [13], the mechanical-ball milling method [26], and the chemical vapor deposition method [27]. In the coprecipitation method, the effect of the ratio of the starting reagents ($ZnSO_4$/$SnCl_4$) [16], the selection of alkaline (NaOH and $NH_3 \cdot H_2O$) [15], and the annealing temperature on photocatalytic activities of coupled semiconductor system have been studied [10,15,17]. In the hydrothermal method, the hydrothermal temperature and time were found to influence the size and morphology of ZnO-SnO_2 coupled semiconductor particles, which in turn results in different photocatalytic activities [11]. Therefore, enhanced photocatalytic activity can be obtained by coupling the different semiconductors and controlling the experimental parameters in the synthesis process.

In contrast to the coupled semiconductor system, loading noble metals on the surface of semiconductor to trap the charge carriers has been reported as another important method to improve the photocatalytic activity of semiconductor [7,28–35]. Various noble metal-loaded semiconductor systems, including Ag, Pt, Au/ZnO [7,28–32], and Ag, Pt, Au/TiO_2 [33–35], have been studied. The kind, size and amount of noble metal loaded on the surface of semiconductor particles were the major factors that affected the photocatalytic activities of semiconductor [7,29]. Consequently, the improved photodegradation efficiency can be obtained by controlled synthesis of a noble metal-loaded system [7,29]. In par-

* Corresponding author. Tel.: +82 2 2123 5754; fax: +82 2 312 6401.
E-mail address: swlim@yonsei.ac.kr (S. Lim).

1385-8947/$ – see front matter © 2008 Elsevier B.V. All rights reserved.
doi:10.1016/j.cej.2008.06.016

ticular, whether Ag-loaded ZnO catalysts were synthesized through an one-step flame spray pyrolysis, simple coprecipitation [30], or the solvothermal method [31], Ag-loading on ZnO catalysts exhibited improved photocatalytic activity [29–31].

While coupling semiconductors or loading noble metals have been shown to exhibit a beneficial influence on the photocatalytic activity of semiconductor, there is no direct evidence for the possibility of further improving the photocatalytic property of coupling semiconductor system or noble metal-loaded semiconductor system. Recent studies have reported hydrogen production through partial oxidation of methanol over gold catalysts by using a composite support CuO/ZnO or MO_x (M = Fe, Co, Zn)/TiO_2 system [36,37]. Such a composite system has been verified to be active for hydrogen production. Unfortunately, in the research of semiconductor photocatalysis, most studies have been concerned with either coupling semiconductor or noble metal loading alone. Studies considering the possible benefits of combining coupling semiconductors and noble metal loading are much less common. In the present study, the Ag-loaded ZnO-SnO_2 coupled semiconductor has been prepared through the coprecipitation method. The photocatalytic activity of Ag/ZnO-SnO_2 was studied using methyl orange as a model organic pollutant. In addition, the effects of the pH value of the solution used to synthesize the ZnO-SnO_2 coupled semiconductor and the annealing temperature for calcination were evaluated. The present study aims to prepare an Ag/ZnO-SnO_2 semiconductor system and to characterize this new composite material and its photocatalytic activities in contrast to ZnO-SnO_2 coupled semiconductors and noble metal-loaded Ag/ZnO catalysts.

2. Experimental

2.1. Preparation of Ag/ZnO-SnO_2 catalysts

ZnO-SnO_2 coupled semiconductor nanoparticles were prepared by the coprecipitation method, which is similar to that reported in the literature [10]. Zinc sulfate hydrate ($ZnSO_4{\cdot}7H_2O$, 99%, Aldrich) and tin chloride hydrate ($SnCl_4{\cdot}5H_2O$, Aldrich) were used as zinc and tin precursors without further purification. $ZnSO_4{\cdot}7H_2O$ and $SnCl_4{\cdot}5H_2O$ in the molar ratio 2:1 were dissolved in 500 mL deionized water. Then, lithium hydroxide monohydrate ($LiOH{\cdot}H_2O$, 99%, Aldrich) was added into the solution as the coprecipitant to adjust the pH value to 7 and 10, respectively. The solution was agitated by a magnetic bead for 30 min at 60 °C. During this process, the solution became milky white, as the white precipitates were slowly formed. After the solution was cooled down to room temperature, the precipitates were separated from the solution by centrifugation, and washed with deionized water three times in order to eliminate SO_4^{2-} and Cl^- ions on the surface of precipitates. The wet precipitates were dried in an oven at 100 °C. Finally, two different ZnO-SnO_2 coupled semiconductor precursors were synthesized at pH 7 and 10. After annealing at 600 °C for 2 h, two kinds of precursors were transformed into coupled ZnO-SnO_2 catalysts, labeled ZS7 and ZS10, respectively. They were also used as the bulk materials for preparing Ag-loaded ZnO-SnO_2 catalysts.

The preparation of the Ag/ZnO-SnO_2 catalysts was carried out according to the procedure reported in the literature elsewhere [29]. Two grams of ZnO-SnO_2 precursor prepared at pH 7 and 5 mL of $AgNO_3$ solution with variable concentration were mixed in a beaker by agitating with a glass tube. Then the beaker was moved to the oven and the mixture was dried at 110 °C for 30 min to obtain the composite powders. The powders were subjected to calcination for 2 h at 400, 600, and 800 °C, to get Ag/ZnO-SnO_2 powders with different Ag loadings (1, 3, and 5%, respectively). The three loaded powders were labeled 1%Ag/ZS7, 3%Ag/ZS7, and 5%Ag/ZS7. For comparison, pure ZnO powders were synthesized with zinc sulfate hydrate by the same procedure described above. The pure ZnO powders prepared at pH 7 and 10 were labeled Z7 and Z10, respectively. In addition, a 3% Ag-loaded ZnO system synthesized at pH 7 and labeled 3%Ag/Z7, was also prepared.

2.2. Photocatalytic experimental of Ag/ZnO-SnO_2 catalysts

The photocatalytic experiments were conducted in a 500 mL beaker under the illumination of a single UV light lamp (UVITEC, UVIlite LF215LS), which predominantly emits at 365 nm with a definite power of 15 W. For each condition, the reaction suspension was prepared by adding 200 mg catalysts into a 100 mL methyl orange solution with an initial concentration of 10 mg/L. The suspension was subjected to ultrasonic dispersion for 15 min, and then magnetically stirred for 30 min in the dark to ensure the equilibrium of absorption/desorption between dye molecules and photocatalysts. Next, the suspension was irradiated by the UV lamp. During the photodegradation process, the UV lamp was positioned horizontally above the surface of the suspension. The distance between UV lamp and the surface was set at 10 cm.

Analytical samples were taken out for measurement after various reaction times. The degradation efficiency of different photocatalysts was analyzed by UV–vis spectrophotometer (Optizen 2120UV) at its maximum absorption wavelength of 465 nm. The degradation efficiency as a function of reaction time was calculated by the concentration ratio of the original and analytical samples.

2.3. Characterization of Ag/ZnO-SnO_2 catalysts

The catalysts were measured by a high resolution transmission electron microscope (HRTEM, JEOL, JEM-3010) combined with energy dispersive spectroscopy (EDS, Oxford) using an accelerating voltage of 300 kV. X-ray diffraction patterns were obtained using a Mini X-ray diffractometer with Cu $K\alpha_1$ radiation at a scanning speed of $2^\circ\ min^{-1}$. Diffuse reflectance spectra of the catalysts were recorded with a UV–vis spectrophotometer (SCLNCO S-3100) in the wavelength range of 300–800 nm. Specific surface areas of the samples were characterized with the Brunauer–Emmet–Teller (BET) method using a Tristar 3000 gas (N_2) analyzer.

3. Results and discussion

3.1. Characterization of ZnO-SnO_2 coupled photocatalysts

Fig. 1 shows the XRD patterns of the ZnO and ZnO-SnO_2 coupled oxide powders annealed at 600 °C for 2 h. For the pure ZnO powders (Z7 and Z10), all the diffraction peaks can be indexed as the typical hexagonal wurtzite with lattice constants in agreement with the values in the standard card (JCPDS 36-1451). No other diffraction peaks are detected in the pure ZnO powders. However, the XRD patterns of the coupled oxides (ZS7 and ZS10) consist of the individual components of ZnO and SnO_2. The broadness of the SnO_2 phase peaks is much wider than that of the ZnO diffraction peaks, which indicates the smaller size of the SnO_2 crystal in the coupled oxide powders. When the pH value is increased from 7 to 10, no significant phase changes are observed for both pure and coupled oxide powders.

Fig. 2 shows the TEM images of as-prepared ZnO (Fig. 2(a) and (b)) and ZnO-SnO_2 coupled oxide powders (Fig. 2(c) and (d)). It can easily be seen that the pure ZnO powders consist of irregular particles around 100–150 nm, while the coupled oxide consists of particles around 10–30 nm. Due to aggregation, the SnO_2 and ZnO particles are not distinguishable from each other. Therefore, the mean sizes of SnO_2 and ZnO were calculated by Scherrer Formula

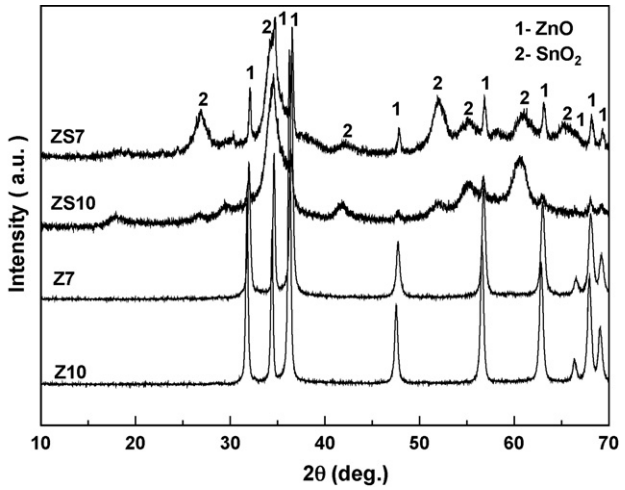

Fig. 1. XRD patterns of pure ZnO and ZnO-SnO_2 coupled oxide powders.

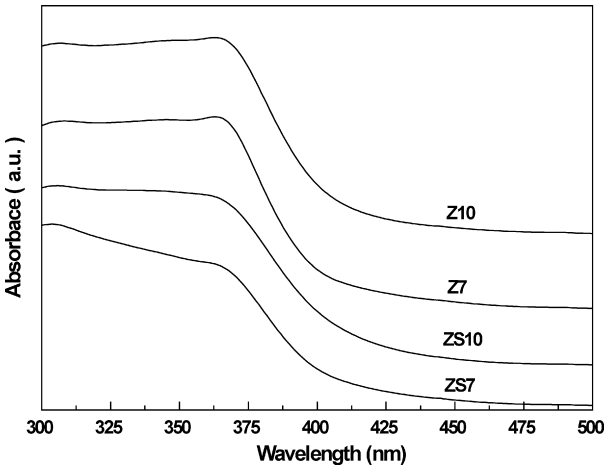

Fig. 3. UV–vis absorbance spectra of pure ZnO and ZnO-SnO_2 coupled oxide powders.

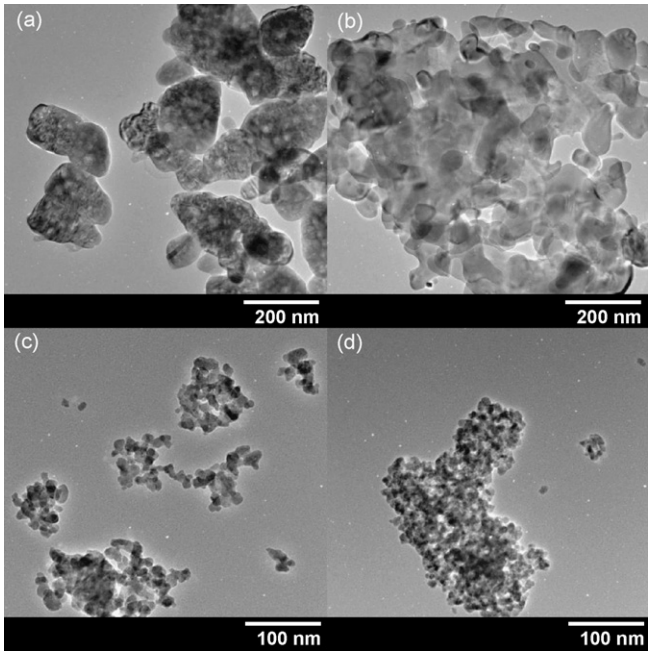

Fig. 2. TEM images of pure ZnO and ZnO-SnO_2 coupled oxide powders. (a) Z10, (b) Z7, (c) ZS10, and (d) ZS7.

by selecting each (1 0 1) and (1 1 0) crystal plane, respectively. The detailed size and surface area information of photocatalysts is listed in Table 1. With an increase of pH value from 7 to 10, the mean size of the ZnO particles increased from 100 to 150 nm, which is consistent with previous reports [38,39]. This may result from the increase in zinc hydroxide concentration in the bulk solution [38], and/or agglomeration of ZnO nanoparticles, when the pH of the solution increases [39]. From BET measurements, the decrease in surface area of the powders from 7.3736 to 4.0904 m^2/g is observed. However, it is strange for ZnO-SnO_2 coupled oxide powders to abruptly increase in surface area from 25.8169 to 52.5028 m^2/g when pH value is increased from 7 to 10. It should be noted that the pH value does not significantly affect the mean sizes of ZnO and SnO_2 in the coupled oxide powders (see Table 1). It has been reported that the specific surface area increased with the increase of Sn content up to 66.7 mol% for ZnO-SnO_2 coupled oxide powders [16]. Therefore, it can be suggested that the increase of surface area from pH 7 to 10 observed in the present study may result from an increased ratio of SnO_2 to ZnO in the coupled oxide powders. For all the samples, the size of ZnO is larger than that of SnO_2, which may result from the fact that ZnO particles are inclined to grow bigger more easily under annealing than SnO_2 particles [40]. Furthermore, the size of ZnO in coupled oxide powders is much smaller than in pure ZnO powders, which is consistent with the previous study that the addition of SnO_2 hinders the growth of ZnO crystal [41].

UV–vis absorbance spectra for pure ZnO and ZnO-SnO_2 coupled oxide powders are shown in Fig. 3. In general, the sharp UV–vis absorption curve of samples indicates good crystalline quality [29]. From Fig. 3, it is observed that the UV–vis absorption curves of pure ZnO powders are sharper than those of the coupled oxide powders, which indicates the higher crystalline quality of pure ZnO powders. The band gap energy was calculated by determining the absorption edges of different oxide powders [42], as shown in Table 1. The band gap energy of coupled oxide powders is lower than that of pure ZnO powders. For the coupled oxide powders, the band gap energy arises from the synergistic effect of ZnO and SnO_2 [11,42]. A SnO_2 semiconductor has an indirect band gap energy of 2.6 eV [43], which may be the reason that the band gap energy decreases when the ZnO particles are coupled with SnO_2 powders. In addition, it was reported that the band gap energy of coupled oxide powders decreased with a higher Sn content [16]. The decrease in band gap energy is also observed when the oxide powders were prepared at a higher pH value. The lower band gap energy for the sample prepared at pH 10 may result from a higher Sn content in the powders. In conclusion, TEM, XRD, BET and UV–vis DRS results demonstrate

Table 1
The microstructural characteristics of pure ZnO and ZnO-SnO_2 coupled oxide powders

Sample	Mean size of ZnO (nm)	Mean size of SnO_2 (nm)	Surface area (m_2/g)	Absorption wavelength (nm)	Band gap energy (eV)
Z10	150	–	4.0904	404	3.07
Z7	100	–	7.3736	399	3.11
ZS10	32	5	52.5028	410	3.02
ZS7	30	6	25.8169	406	3.05

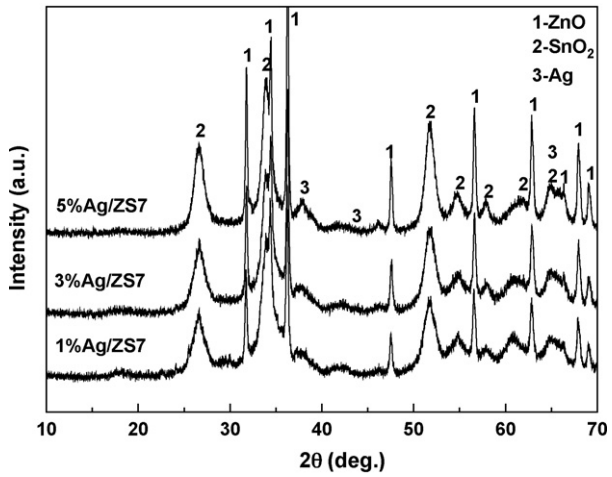

Fig. 4. XRD patterns of Ag-loaded ZS7 catalysts.

that the pH value influences the size of the pure ZnO powders, the ratio of SnO_2 to ZnO, and the band gap energy of the coupled oxide powders.

3.2. Ag/ZnO-SnO_2 characterization

Fig. 4 shows the XRD patterns of ZS7 photocatalysts with different Ag loadings after annealing at 600 °C. The diffraction peaks of ZnO, SnO_2, and Ag are observed for the Ag-loaded ZnO-SnO_2 coupled semiconductor catalysts. No silver oxide diffraction peaks are found in the patterns, indicating that the silver has been formed through the calcinations. For 1%Ag/ZnO-SnO_2 catalyst, the signals of silver species are not obvious, which can be attributed to the low silver content and the high dispersion of silver particles on the coupled oxide supports. However, with the increase of silver loading, the silver particles agglomerated in accordance with the sharper silver diffraction peaks.

XRD patterns of 3%Ag/ZS7 annealed at 400 and 800 °C are shown in Fig. 5. It is reported that crystalline ZnO-SnO_2 coupled oxide powders can be obtained only at an annealing temperature above 300 °C for 2 h [17]. However, from Fig. 5, it is observed that calcination at a temperature above 400 °C is needed for the formation of crystalline SnO_2 in our present work. In addition, no diffraction

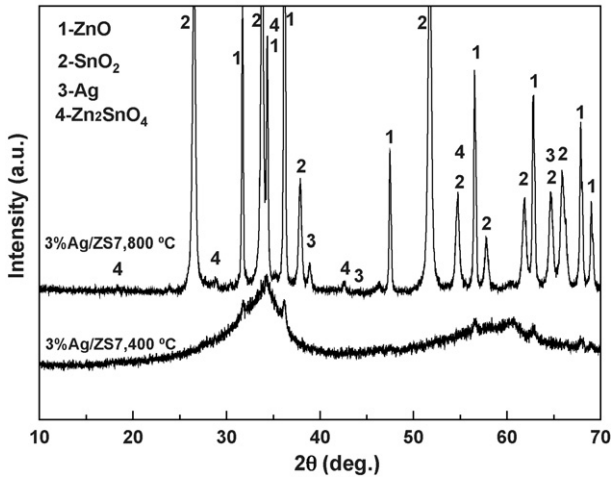

Fig. 5. The effect of annealing temperature on the XRD patterns of 3%Ag/ZS7 catalysts.

peak representing for silver is obtained in the XRD pattern when the annealing temperature is 400 °C. When the annealing temperature is increased to 600 °C (see Fig. 4), the crystalline SnO_2 and Ag do form. With a further increase of the annealing temperature to 800 °C, a new spinel-type Zn_2SnO_4 type is formed, which originates from the solid reaction between ZnO and SnO_2 [44]. However, the lower peak intensity of Zn_2SnO_4 represents its lower content than ZnO and SnO_2 in the powders. In addition, the diffraction peaks of ZnO and SnO_2 become sharper, indicating the increase of crystal size and improvement of crystallinity. The specific surface areas of 3%Ag/ZnO-SnO_2 annealed at 400, 600, and 800 °C were measured to be 40.9766, 24.5230, and 6.2309 m^2/g, respectively.

Fig. 6 shows the TEM images and EDS spectra of Ag-loaded ZS7 photocatalysts. From TEM images, it is observed that the amount of silver loading has little influences on the size and distribution of the coupled photocatalysts. From the EDS elemental composition signals, Zn, Sn, and O elements have been observed. No apparent peaks of silver can be observed at low concentration of silver loading (1%). However, when the silver loading is increased to 3%, the diffraction peaks of silver become obvious and sharper. The intensity is further increased when the silver loading reaches 5%.

On the other hand, the absorption wavelengths of UV–vis spectra for Ag-loaded ZS7 samples were characterized to be 402–403 nm regardless of Ag loading amount (data not shown), exhibiting a slight blue shift in contrast to ZnO-SnO_2 powders without silver loading (406 nm). Not only the silver loading, but also the annealing temperature affects the absorption wavelength. The absorption wavelength of 3%Ag/ZS7 was increased from 401 to 405 nm when the annealing temperature was increased from 400 to 800 °C, which is similar to the previous study [15]. It is known that the band gap energy of the semiconductor is related to the photocatalytic activity of the catalysts [1]. The larger band gap energy indicates the greater redox capacity of the catalysts [1]. Therefore, it is suggested that the amount of silver loading and the temperature of annealing have a great impact on the redox capacity of catalysts to photogenerate more electron–hole pairs in the photocatalytic process.

3.3. Photocatalytic activities of the catalysts

3.3.1. Effect of pH value on the activities of coupled photocatalysts

Fig. 7 shows the degradation rate of methyl orange over ZnO and ZnO-SnO_2 catalysts prepared at different pH values. The catalysts prepared at pH 7 exhibit higher photocatalytic activity than those prepared at pH 10. The higher electrostatic repulsion between the methyl orange anion (pK_1 = 3.46) and the highly negative charged oxide surface deteriorates the activity of catalysts [10]. Therefore, in the present study, it is suggested that the pH value in the synthesis process of the catalysts affects the charged situation of catalysts' surface, which in turn influences the adsorption of the anion. A higher pH value may induce the formation of a highly negatively charged oxide surface, which weakens the photocatalytic activity.

From Fig. 7, it is also noted that the degradation rate for coupled oxide powders prepared at pH 7 is higher than that of pure ZnO powders prepared at the same pH level. This would be ascribed to the hetero-junctions of ZnO-SnO_2, which would effectively separate the photogenerated electron–hole pairs. However, it is interesting that the coupled catalyst prepared at pH 10 exhibits a lower photocatalytic activity than the pure ZnO powders synthesized at the same pH value, although it has a larger surface area (see Table 1). The previous study demonstrated that the photocatalytic activity of coupled oxide powders is closely related to the ratio of the two oxides [16,18,19]. Therefore, it is suggested that the higher ratio of SnO_2 in the catalysts prepared at pH 10 may be harmful

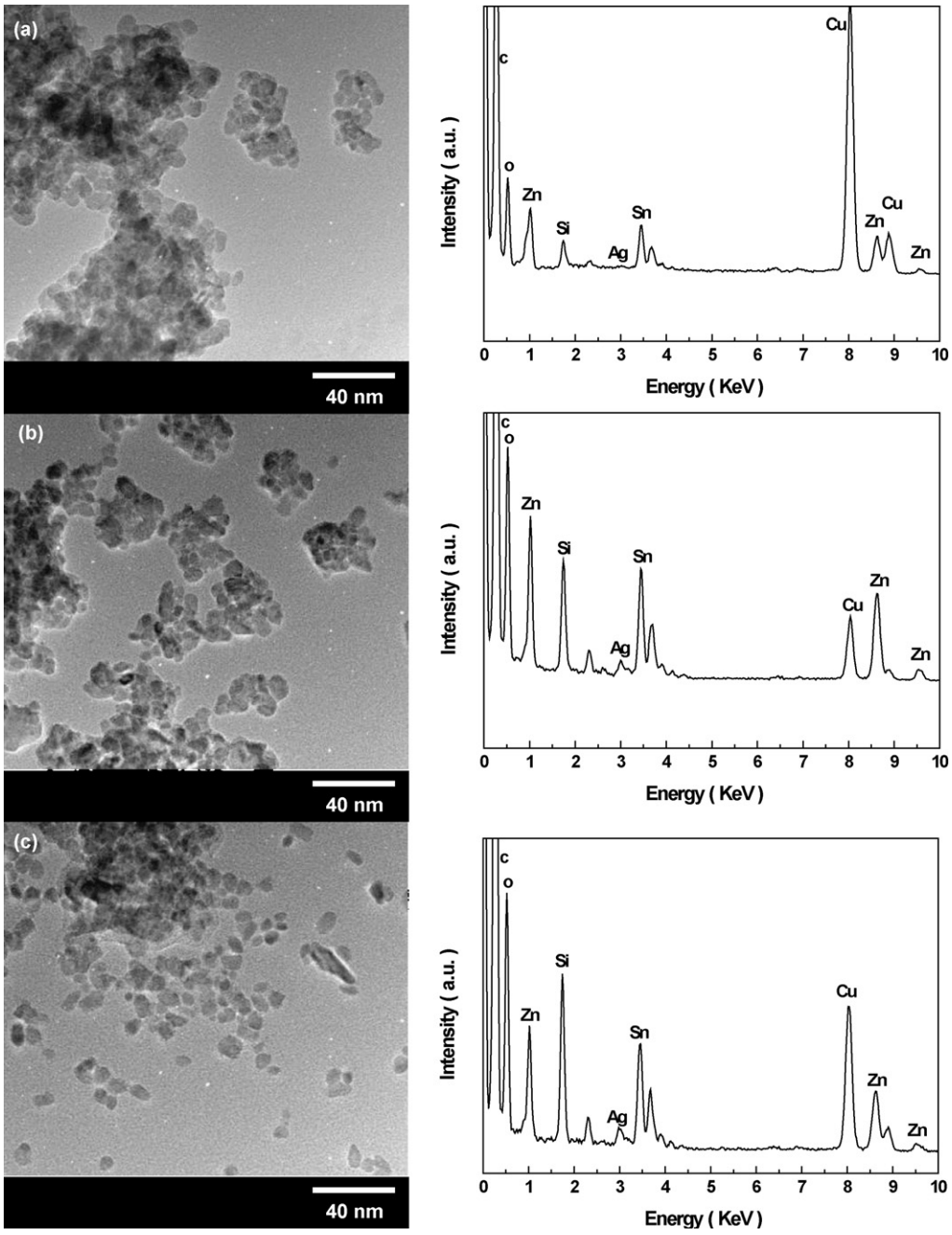

Fig. 6. TEM images and EDS spectra of Ag-loaded ZS7 catalysts. (a) 1%Ag/ZS7, (b) 3%Ag/ZS7, and (c) 5%Ag/ZS7.

to the overall photocatalytic activity because of its intrinsic low photocatalytic capability.

3.3.2. *Effect of silver loading on the activities of coupled photocatalyst*

The effect of Ag loading on the photocatalytic activity of ZnO-SnO_2 coupled oxide powders is shown in Fig. 8. The degradation of methyl orange for Ag-loaded ZS7 catalysts was monitored to measure the photocatalytic activity. For the catalysts annealed at 600 °C, the photocatalytic activity increased with the increase of Ag loading from 1 to 5%. The improvement of photocatalytic activity by Ag loading is attributed to the alignment of the Fermi levels of the silver and the semiconductor, which makes the electrons flow to the silver from semiconductors, thus resulting in the effective separation of the generated electron–hole pairs [3]. However, the performance of the 5%Ag/ZnO-SnO_2 does not show as great an improvement as that of the 3%Ag/ZnO-SnO_2. This may be due to the agglomeration of silver particles, which reduces the chances of silver particles attaching on the surface of the semiconductor. Therefore, 3%Ag is suggested as the optimal loading amount, to limit the consumption of $AgNO_3$ chemicals in the synthesis process.

Fig. 8 also demonstrates the effect of annealing temperature on the activity of 3% Ag-loaded ZS7 catalysts. The catalyst annealed at 600 °C shows the highest conversion performance, while the catalyst annealed at 400 °C exhibits the lowest performance. The decrease in the performance of catalyst annealed at 400 °C may be attributed to its unmatured crystallinity, as shown in Fig. 5. Although there is no signal of Ag in the XRD pattern at 400 °C (see

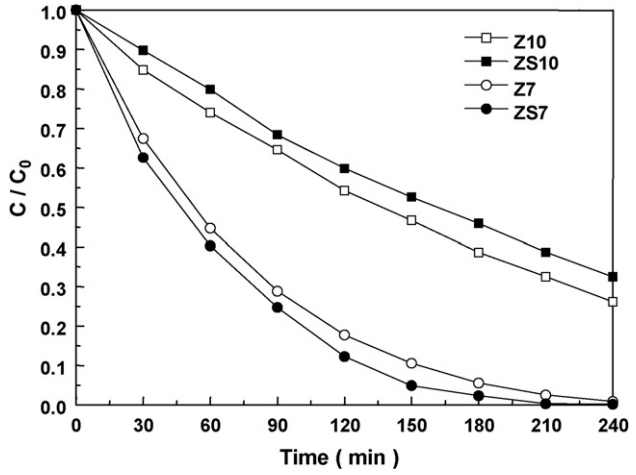

Fig. 7. Photodegradation of methyl orange solution using pure ZnO and ZnO-SnO_2 coupled oxide powders annealed at 600 °C.

Fig. 5), Ag particles will be formed from silver ions during the UV irradiation in the photocatalytic process for photoreduction [45], improving the performance of catalysts. For the catalysts annealed at 800 °C, the decrease of the surface area and the formation of Zn_2SnO_4 may degrade its photocatalytic activity greatly.

For comparison, pseudo first-order rate constants of Z7, ZS7, 3%Ag/Z7, and 3%Ag/ZS7 catalysts are shown in Fig. 9. The rate constant of 3%Ag/ZS7 is higher than that of 3%Ag/Z7, ZS7, and Z7 by 33, 84, and 88%, respectively. In this study, it is found that silver loading improves the photocatalytic activity of ZnO catalysts compared to coupling SnO_2 on ZnO support. In addition, the combinative role of silver loading and coupling of SnO_2 on ZnO support is observed. As previously mentioned, the ZnO-SnO_2 hetero-junctions would improve the performance of the coupled oxide catalysts. However, there will be conflicting factors which will suppress the photocatalytic activity of coupled catalysts, such as the aggregation of ZnO particles without attachment of SnO_2, and the aggregation between SnO_2. To remove those conflicting factors, Ag particles were deposited on the surface of ZnO-SnO_2 hetero-junctions and each of the ZnO and SnO_2 aggregates. The Ag particles loaded on the surface of ZnO and SnO_2 aggregates may act as the trapper of photogenerated electrons to enhance the conversion performance. In addition, it is suggested that the photocatalytic activity of ZnO-SnO_2 hetero-junctions would not be damaged by Ag loading, which may result from the fact that photogenerated electrons have one more channel for being effectively separated from the electron–hole pairs. Therefore, the conflicting factors in the coupled oxide catalyst can be improved by Ag loading. As a result, the Ag-loaded coupled semiconductor photocatalyst exhibits the highest photocatalytic activity as compared to ZnO-SnO_2 coupled semiconductor and Ag-loaded ZnO catalyst.

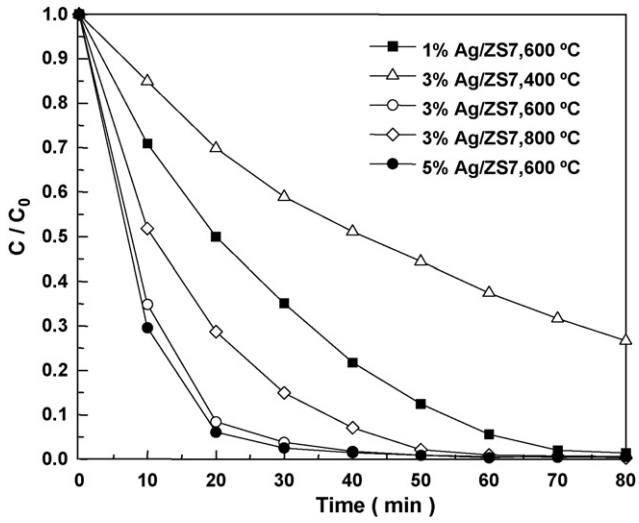

Fig. 8. Effects of silver loading and annealing temperature on the photocatalytic activity of Ag-loaded ZS7 catalysts.

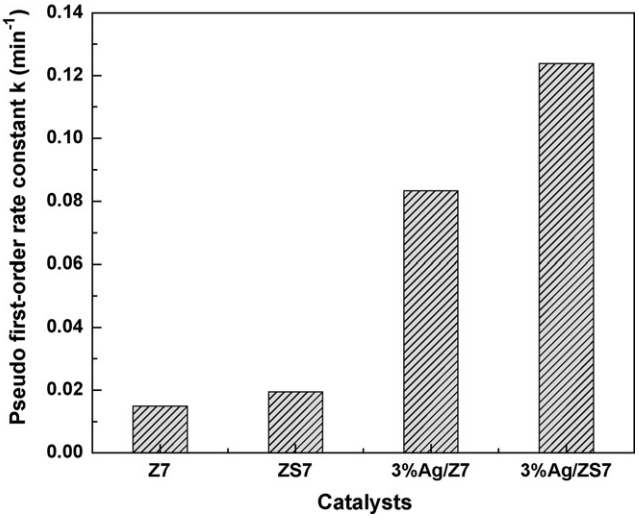

Fig. 9. Pseudo first-order rate constants of catalysts Z7, ZS7, 3%Ag/Z7 and 3%Ag/ZS7.

4. Conclusions

ZnO-SnO_2 coupled oxide powders were prepared through coprecipitation method at pH 7 and 10. It was found that pH value has a little influence on the size of catalysts. However, the ratio of SnO_2 to ZnO in the coupled oxide powders increased with the increase of pH value from 7 to 10. The coupled catalyst prepared at pH 7 exhibited a better activity than that prepared at pH 10 for the appropriate ratio of ZnO-SnO_2.

The Ag-loaded ZnO-SnO_2 catalysts were synthesized using coupled oxide powders prepared at pH 7 as support. With the increase of Ag loading from 1 to 5%, the photocatalytic activity was improved. However, 5%Ag/ZS7 catalyst exhibited a little higher photocatalytic activity than 3%Ag/ZS7, which demonstrates that the optimum Ag loading is around 3%, considering the consumption of $AgNO_3$ chemicals. The photocatalytic experiments also show that 3%Ag/ZS7 catalyst annealed at 600 °C with a high specific surface area and crystallinity has the fastest photodegradation rate of methyl orange as compared to that annealed at 400 °C and 800 °C. In addition, the pseudo first-order rate constant of 3%Ag/ZS7 was higher than that of 3%Ag/Z7, ZS7, and Z7 by 33, 84, and 88%, respectively. The highest photocatalytic activity of 3%Ag/ZS7 is likely ascribed to the dual role of noble metal loading and coupling semiconductor to separate photogenerated electron–hole pairs more effectively.

References

[1] A. Hagfeldt, M. Graetzel, Light-induced redox reactions in nanocrystalline systems, Chem. Rev. 95 (1995) 49–68.
[2] M.R. Hoffmann, S.T. Martin, W. Choi, D.W. Bahnemann, Environmental applications of semiconductor photocatalysis, Chem. Rev. 95 (1995) 69–96.
[3] A.L. Linsebigler, G. Lu, J.T. Yates, Photocatalysis on TiO_2 surfaces: principles, mechanisms, and selected results, Chem. Rev. 95 (1995) 735–758.
[4] S. Rengaraj, S. Venkataraj, J.-W. Yeon, Y. K, X.Z. Li, G.K.H. Pang, Preparation, characterization and application of Nd–TiO_2 photocatalyst for the reduction

of Cr(VI) under UV light illumination, Appl. Catal. Environ. 77 (2007) 157–165.
[5] D. Robert, Photosensitization of TiO_2 by M_xO_y and M_xS_y nanoparticles for heterogeneous photocatalysis applications, Catal. Today 122 (2007) 20–26.
[6] L. Jing, H. Fu, B. Wang, D. Wang, B. Xin, S. Li, J. Sun, Effects of Sn dopant on the photoinduced charge property and photocatalytic activity of TiO_2 nanoparticles, Appl. Catal. B: Environ. 62 (2006) 282–291.
[7] L. Jing, D. Wang, B. Wang, S. Li, B. Xin, H. Fu, J. Sun, Effects of noble metal modification on surface oxygen composition, charge separation and photocatalytic activity of ZnO nanoparticles, J. Mol. Catal. A: Chem. 244 (2006) 193–200.
[8] D. Li, H. Haneda, N. Ohashi, S. Hishita, Y. Yoshikawa, Synthesis of nanosized nitrogen-containing MO*x*–ZnO (M = W, V, Fe) composite powders by spray pyrolysis and their visible-light-driven photocatalysis in gas-phase acetaldehyde decomposition, Catal. Today 93–95 (2004) 895–901.
[9] D. Li, H. Haneda, Photocatalysis of sprayed nitrogen-containing Fe_2O_3–ZnO and WO_3–ZnO composite powders in gas-phase acetaldehyde decomposition, J. Photochem. Photobiol. A: Chem. 160 (2003) 203–212.
[10] C. Wang, J. Zhao, X. Wang, B. Mai, G. Sheng, P. Peng, J. Fu, Preparation, characterization and photocatalytic activity of nano-sized ZnO/SnO_2 coupled photocatalysts, Appl. Catal. B: Environ. 39 (2002) 269–279.
[11] W.-W. Wang, Y.-J. Zhu, L.-X. Yang, ZnO-SnO_2 hollow spheres and hierarchical nanosheets: hydrothermal preparation, formation mechanism, and photocatalytic properties, Adv. Funct. Mater. 17 (2007) 59–64.
[12] Z. Wen, G. Wang, W. Lu, Q. Wang, Q. Zhang, J. Li, Enhanced photocatalytic properties of mesoporous SnO_2 induced by low concentration ZnO doping, Cryst. Growth Des. 7 (2007) 1722–1725.
[13] K. Tennakone, J. Bandara, Photocatalytic activity of dye-sensitized tin(IV) oxide nanocrystalline particles attached to zinc oxide particles: long distance electron transfer via ballistic transport of electrons across nanocrystallites, Appl. Catal. A: Gen. 208 (2001) 335–341.
[14] C. Wang, X. Wang, J. Zhao, B. Mai, G. Sheng, P. Peng, J. Fu, Synthesis, characterization and photocatalytic property of nano-sized Zn_2SnO_4, J. Mater. Sci. 37 (2002) 2989–2996.
[15] M. Zhang, T. An, X. Hu, C. Wang, G. Sheng, J. Gu, Preparation and photocatalytic properties of a nanometer ZnO-SnO_2 coupled oxide, Appl. Catal. A: Gen. 260 (2004) 215–222.
[16] C. Wang, X. Wang, B. Xu, J. Zhao, B. Mai, P. Peng, G. Sheng, J. Fu, Enhanced photocatalytic performance of nanosized coupled ZnO/SnO_2 photocatalysts for methyl orange degradation, J. Photochem. Photobiol. A: Chem. 168 (2004) 47–52.
[17] M. Zhang, G. Sheng, J. Fu, T. An, X. Wang, X. Hu, Novel preparation of nanosized ZnO-SnO_2 with high photocatalytic activity by homogeneous co-precipitation method, Mater. Lett. 59 (2005) 3641–3644.
[18] Y.T. Kwon, K.Y. Song, W.I. Lee, G.J. Choi, Y.R. Do, Photocatalytic behavior of WO_3-loaded TiO_2 in an oxidation reaction, J. Catal. 191 (2000) 192–199.
[19] K.K. Akurati, A. Vital, J. Dellemann, K. Michalow, T. Graule, D. Ferri, A. Baiker, Flame-made WO_3/TiO_2 nanoparticles: relation between surface acidity, structure and photocatalytic activity, Appl. Catal. B: Environ. 79 (2008) 53–62.
[20] I. Bedja, P.V. Kamat, Capped semiconductor colloids: synthesis and photoelectrochemical behavior of TiO_2 capped SnO_2 nanocrystallites, J. Phys. Chem. 99 (1995) 9182–9188.
[21] K. Vinodgopal, P.V. Kamat, Enhanced rates of photocatalytic degradation of an azo dye using SnO_2/TiO_2 coupled semiconductor thin films, Environ. Sci. Technol. 29 (1995) 841–845.
[22] J. Lin, J.C. Yu, D. Lo, S.K. Lam, Photocatalytic activity of rutile $Ti_{1-x}Sn_xO_2$ solid solutions, J. Catal. 183 (1999) 368–372.
[23] K. Vinodgopal, I. Bedja, P.V. Kamat, Nanostructured semiconductor films for photocatalysis: photoelectrochemical behavior of SnO_2/TiO_2 composite systems and its role in photocatalytic degradation of a textile azo dye, Chem. Mater. 8 (1996) 2180–2187.
[24] L. Shi, C. Li, H. Gu, D. Fang, Morphology and properties of ultrafine SnO_2-TiO_2 coupled semiconductor particles, Mater. Chem. Phys. 62 (2000) 62–67.
[25] S. Liao, D. Huang, D. Yu, Y. Su, G. Yuan, Preparation and characterization of ZnO/TiO_2, SO_4^{2-}/ZnO/TiO_2 photocatalyst and their photocatalysis, J. Photochem. Photobiol. A: Chem. 168 (2004) 7–13.
[26] J.F. Wang, Y.J. Wang, W.B. Su, H.C. Chen, W.X. Wang, Novel (Zn, Nb)-doped SnO_2 varistors, Mater. Sci. Eng. B 96 (2002) 8–13.
[27] Q. Kuang, Z.Y. Jiang, Z.X. Xie, S.C. Lin, Z.W. Lin, S.Y. Xie, R.B. Huang, L.S. Zheng, Tailoring the optical property by a three-dimensional epitaxial heterostructure: a case of ZnO/SnO_2, J. Am. Chem. Soc. 127 (2005) 11777–11784.
[28] C.A.K. Gouvea, F. Wypych, S.G. Moraes, N. Duran, P. Peralta-Zamora, Semiconductor-assisted photodegradation of lignin, dye, and kraft effluent by Ag-doped ZnO, Chemosphere 40 (2000) 427–432.
[29] M.J. Height, S.E. Pratsinis, O. Mekasuwandumrong, P. Praserthdam, Ag-ZnO catalysts for UV-photodegradation of methylene blue, Appl. Catal. B: Environ. 63 (2006) 305–312.
[30] G. Zhou, J. Deng, Materials, Preparation and photocatalytic performance of Ag/ZnO nano-composites, Mater. Sci. Semicond. Proc. 10 (2007) 90–96.
[31] T. Chen, Y. Zheng, J.-M. Lin, G. Chen, Study on the photocatalytic degradation of methyl orange in water using Ag/ZnO as catalyst by liquid chromatography electrospray ionization ion-trap mass spectrometry, J. Am. Soc. Mass. Spectrom. 19 (2008) 997–1003.
[32] V. Subramanian, E.E. Wolf, P.V. Kamat, Green emission to probe photoinduced charging events in ZnO-Au nanoparticle: charge distribution and fermi-level equilibration, J. Phys. Chem. B 107 (2003) 7479–7485.
[33] T. Abe, E. Suzuki, K. Nagoshi, K. Miyashita, M. Kaneko, Electron source in photoinduced hydrogen production on Pt-supported TiO_2 particles, J. Phys. Chem. B 103 (1999) 1119–1123.
[34] V. Subramanian, E. Wolf, P.V. Kamat, Semiconductor–metal composite nanostructures: to what extent do metal nanoparticles improve the photocatalytic activity of TiO_2 films, J. Phys. Chem. B 105 (2001) 11439–11446.
[35] W.Y. Teoh, L. Madler, D. Beydoun, S.E. Pratsinis, R. Amal, Direct (one-step) synthesis of TiO_2 and Pt/TiO_2 nanoparticles for photocatalytic mineralisation of sucrose, Chem. Eng. Sci. 60 (2005) 5852–5861.
[36] H.-C. Yang, F.-W. Chang, L.S. Roselin, Hydrogen production by partial oxidation of methanol over Au/CuO/ZnO catalysts, J. Mol. Catal. A: Chem. 276 (2007) 184–190.
[37] F.-W. Chang, H.-Y. Yu, L.S. Roselin, H.-C. Yang, T.-C. Ou, Hydrogen production by partial oxidation of methanol over gold catalysts supported on TiO_2–MO_x (M = Fe, Co, Zn) composite oxides, Appl. Catal. A: Gen. 302 (2006) 157–167.
[38] C.-H. Lu, C.-H. Yeh, Influence of hydrothermal conditions on the morphology and particle size of zinc oxide powder, Ceram. Int. 26 (2000) 351–357.
[39] A.A. Ismail, T.A. El-Midany, E.A. Abdel-Aal, H. El-Shall, Application of statistical design to optimize the preparation of ZnO nanoparticles via hydrothermal technique, Mater. Lett. 59 (2005) 1924–1928.
[40] J.H. Yu, G.M. Choi, Electrical and CO gas-sensing properties of ZnO/SnO_2 heterocontact, Sens. Actuators B: Chem. 61 (1999) 59–67.
[41] J.H. Yu, G.M. Choi, Electrical and CO gas sensing properties of ZnO-SnO_2 composites, Sens. Actuators B: Chem. 52 (1998) 251–256.
[42] P.L. Provenzano, G.R. Jindal, J.R. Sweet, W.B. White, Flame-excited luminescence in the oxides Ta_2O_5, Nb_2O_5, TiO_2, ZnO, and SnO_2, J. Lumin. 92 (2001) 297–305.
[43] W. Spence, The UV absorption edge of tin oxide thin films, J. Appl. Phys. 38 (1967) 3767–3770.
[44] T. Hashemi, H.M. Al-allak, J. Illingsworth, A.W. Brinkman, I. Woods, Sintering behavior of zinc stannate, J. Mater. Sci. Lett. 9 (1990) 776–778.
[45] S. Chen, U. Nickel, Controllable exciton bleaching and recovery observed in ZnO-Ag hybrid nanometre-sized particles, Chem. Commun. 1996 (1996) 133–134.